Chinese Chemical Letters 34 (2023) 107363

Contents lists available at ScienceDirect

Chinese Chemical Letters

journal homepage: www.elsevier.com/locate/cclet

Monolithic polyimine vitrimer/graphene aerogel composites

Jinye Zhang[a,1], Shichang Luo[a,1], Yunlong Ma[a], Ruiyang Li[a], Yinghua Jin[b], Li Qiu[a,*], Wei Zhang[b,*]

[a] Yunnan Key Laboratory for Micro/Nano Materials & Technology, National Center for International Research on Photoelectric and Energy Materials, School of Materials and Energy, Yunnan University, Kunming 650091, China
[b] Department of Chemistry, University of Colorado Boulder, Boulder, CO 80309, United States

ARTICLE INFO

Article history:
Received 8 December 2021
Revised 13 March 2022
Accepted 21 March 2022
Available online 24 March 2022

Keywords:
Vitrimer
Graphene aerogel
Polyimine
Rehealable
Piezoresistive
Monolithic

ABSTRACT

Graphene-polymer composites have attracted great attention as sensing materials due to their tailorable electrical conductivity, physicochemical properties, and sensitivity to geometric and functional changes. Herein, we report the first example of cylindrical monolithic polyimine vitrimer/graphene composites with excellent mechanical, compressive, rehealable and recyclable, and piezoresistive properties *via* simple infiltration of polymer monomers into the pores of graphene aerogel followed by thermal curing. The composites exhibit excellent durable compressibility (negligible reduction in the compression properties even after 3000 consecutive compression cycles), rapid recovery to the original size upon stress released, high compressive strength (up to 1.2 MPa), and high conductivity (up to 79 S/m). Excellent piezoresistive properties were observed, displaying consistent and reliable change of the electrical resistance with the compression ratio. Furthermore, rehealing with ~100% recovery of the compressive strength and electric conductivity was achieved under mild rehealing conditions, which is highly desired but has rarely been reported for electronic materials. The facile strategy for fabrication of rehealable monolithic polymer/GAs can open new possibilities for the sustainable development of composites with high electrical conductivity for various applications such as sensing, health monitoring, and movement detection.

Graphene aerogel (GA), one of the existing forms of graphene, not only possesses the attractive intrinsic properties of individual graphene sheet, but also features low density, superior elasticity, and hierarchically porous architecture. Given these unique properties, GA has been widely used in a broad range of applications, such as electrode materials for energy storage/conversion devices [1–4], gas sensors/electronics [5–7], electromagnetic wave absorbing materials [8–10] and environmental protections [11,12]. Given the high electrical conductivity, good compressibility and high porosity, GA has been envisioned as an excellent filler for conductive composites, which can be used as sensing materials.

The three-dimensional (3D) porosity of GAs is formed by curling and stacking two-dimensional (2D) graphene nanosheets. GAs thus have hierarchical micro-, meso– and macro-pores. Various composites of GAs and polymer materials have been fabricated, *e.g.*, infiltration of poly(dimethylsiloxane) [13], epoxy [14] or polyimide [15] monomers into the pores of GAs followed by curing to fabricate monolithic and conductive nanocomposites, or co-assembly through either covalent bonds or noncovalent interactions to produce 3D GA/polymer composites [16]. However, most of the above-mentioned GA composites exhibit low mechanical properties and durability and also are not reprocessable or repairable, which severely limits their applications. Furthermore, to reduce environmental impact and manufacturing cost, more sustainable approaches are expected.

Polyimine (PI), a type of vitrimers (also called covalent adaptable networks) [17–20], could be employed as a polymer matrix. The advantage of using PI vitrimers is their malleability and corresponding thermal drive, *i.e.*, under heating conditions, reversible imine bonds in the cross-linked network can be activated, thus changing the topology of the network. The imine bonds could be deactivated upon cooling, which can freeze the topology of the material. Such reversibly activated/deactivated state of imine bonds enables the malleability, repairability, and easy recovery/recyclability of the materials [21–23]. Herein, we report the first example of rehealable and recyclable cylindrical monolithic PI and GA composites (denoted as mPI-aGAs), which exhibit excellent piezoresistive property (*i.e.*, sensitive, repeatable and durable) with high compressive strength of up to 1.2 MPa and high conductivity of up to 79 S/m. The composites show excellent durable

* Corresponding authors.
E-mail addresses: qiuli@ynu.edu.cn (L. Qiu), wei.zhang@colorado.edu (W. Zhang).
[1] These authors contributed equally to this work.

https://doi.org/10.1016/j.cclet.2022.03.086
1001-8417/

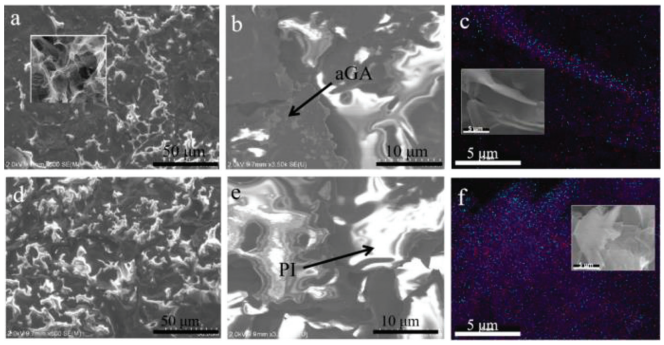

Fig. 1. (a, b, and the inset in c) SEM views of a vertical section and (d, e, and the inset in f) horizontal section with different magnifications of mPI_{60}-aGA_9. The inset in (a) is the SEM image of pristine aGA. (c, f) The corresponding SEM-mapping images to the insets (purple: C, red: O, cyan: N).

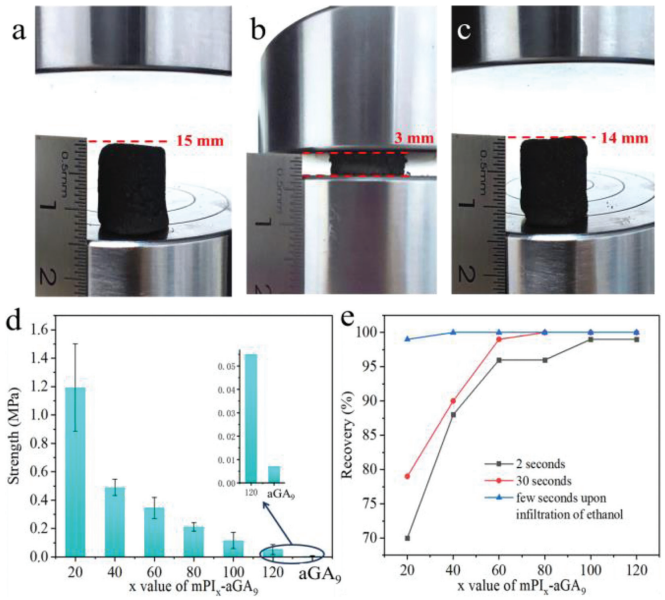

Fig. 2. (a–c) The optical images of mPI_{60}-aGA_9 in a compression cycle. (d) Compressive strength of mPI-aGA_9 and pristine aGA_9 under 50% strain. (e) Compressibility of mPI-aGA within different recovery time.

compressibility with negligible fatigue even after 3000 consecutive compression/release cycles. Furthermore, the composites can be rehealed with nearly 100% recovery of their original properties once the crack of the damaged monolithic composite is repaired. Full recyclability of such composites has also been demonstrated.

Previously, we have demonstrated the use of conductive PI composites with other conductive components integrated, such as silver nanoparticles [24], carbon nanotubes [25] and liquid metal [26] for flexible electronic applications. However, all those composites were prepared as thin films, with the polymer matrix forming a continuous phase while the conductive species added as fillers that are not continuously distributed. Herein, the conductive monolithic PI-GA composites are prepared, with the polymer component continuously wrapped around the "GA matrix", which could maintain the key structural features of GAs, such as superior elasticity, good compressibility, and hierarchically porous architecture, while also bringing in the advantages of PI vitrimer, such as malleability, rehealability and recyclability. As GA is highly porous and could serve as a matrix to incorporate other materials, we prepared conductive monolithic mPI-aGAs using a simple infiltration procedure, *i.e.*, the monolithic annealed (800 °C for 4 h) graphene aerogel (aGA) [27] was soaked in the solution of terephthalaldehyde, diethylenetriamine, and the crosslinker tris(2-aminoethyl)amine in *N,N*-dimethylformamide (DMF). The aGA foam was taken out of the solution after 1, 2 min when white gel (PI with low crosslinking density) started to appear on the surface, then heated gradually using a temperature program (details shown in Experimental procedures in Supporting information) to give the composites. The naming system mPI_x-aGA_y was used for the composites, where x represents the volume of DMF used in the infiltration process (the mmols of the feed monomers are fixed, so a larger x number corresponds to a lower monomer concentration), and y represents the concentration (mg/mL) of GO used in the preparation of GA (a larger y number corresponds to a larger amount of aGA in the composite). The loading of PI in the mPI-aGA could be tuned by varying the concentration of the monomer solution: the larger the volume of the solvent is, the lower the monomer concentration and the loading of PI will be. A series of mPI-aGA composites: mPI_{20}-aGA_9, mPI_{40}-aGA_9, mPI_{60}-aGA_9, mPI_{80}-aGA_9, mPI_{120}-aGA_9, mPI_{60}-aGA_6, mPI_{60}-aGA_{12}, and mPI_{60}-aGA_{15} were obtained following the same procedure. The weight fraction of PI matrix could be as high as 91% (mPI_{20}-aGA_9) using our preparation method.

The SEM images of the composites show that the polyimine distributes in the graphene network in both vertical and horizontal sections of thinly sliced and pressed samples (diameter: 16–20 mm, thickness: 0.6–0.8 mm) as shown in Figs. 1a and d. Higher-magnification SEM images (Figs. 1b–e) and elemental mapping images (insets in Figs. 1c and f) further support that glossy polyimine is wrapped on the surface of graphene sheet. Therefore, the interconnected 3D networks of flexible graphene sheets (Fig. 1a inset) [28] largely retain. It should be noted that the solvent evaporation could cause the de-wetting of solution on GA surfaces, thus uneven distribution of PI on GA (Fig. S1 in Supporting information), which could possibly affect the composite mechanical performance.

The mechanical properties of aGA and mPI-aGA_9 were then evaluated. Although pristine GA can return to its pre-compressed state after removing the relatively low pressure, the compressive strength of pristine GA is still too low to resist high compression and allow fast compression release for practical applications. Under 50% strain, the compressive strength of GA is less than 0.01 MPa, which hardly meets the practical needs, *e.g.*, in the field of tiny wearable devices with a bottom area of ~10–20 mm^2, 0.25 MPa is the lowest limit of compressive strength to withstand 5 N of compressive force without fracturing [29,30]. On the contrary, mPI-aGA composites show greatly enhanced compressibility and mechanical strength [31–34] than that of GA itself, due to the introduction of the elastic polyimine vitrimer component continuously wrapped around the GA matrix (Fig. 2). The compressive strength of the mPI-aGA composite can be as high as 1.2 MPa (for mPI_{20}-aGA_9), which is more than two orders magnitude higher than that of pristine GA (lower than 0.01 MPa) and also significantly higher than the compression strength of other polymer/GA composites, *e.g.*, PDMS/GA [13] and polyimide/GA (<0.2 MPa) [15]. We found the compressive strength (Fig. 2d) and density (Table S1 in Supporting information) of the composites increases with the increase of the weight fraction of PI in the composites: mPI_{120}-aGA_9 (58%) < mPI_{100}-aGA_9 (61%) < mPI_{60}-aGA_9 (72%) < mPI_{40}-aGA_9 (85%) < mPI_{20}-aGA_9 (91%).

Besides the good mechanical strength, mPI-aGA showed excellent compressibility as well. All the mPI-aGAs can be compressed into a pellet under pressure and recovered from the strain almost completely once the external force was removed (Videos S1 and S2 in Supporting information). The instantaneous recovery rates (in ~2 s) are above 70% for all samples. It should be noted that mPI_{60}-aGA_9 recovers >95% in 2 s (Fig. 2e), which makes it suitable

for high frequency applications of repeated compression. When the composite material was left untouched for 30 s, the recovery of mPI_{60}-aGA_9 reached 98%, and the other composites with larger x value all reached ~100%.

Compression is essentially the result of the deformation responses of the 3D pores of GA, which gradually returns to its original size when the stress is removed. Some pores in the pressed state usually cannot naturally recover quickly, but an external force can help with their reopening. Through simple infiltration of a solvent, the pores can be filled to restore the original size of the mPI-aGA (Fig. 2e). We chose ethanol as the candidate as it is relatively environmentally friendly (compared to other organic solvents) and volatile (ethanol adsorbed by mPI-aGA can evaporate naturally in 3 h) [14]. As shown in Video S2, once the pressure is released, the aerogels can spring back immediately to achieve the full height in a few seconds (~5 s). The compressed composite rapidly adsorbs ethanol upon the ethanol-fall and springs back to its original appearance in shape and tunes back to the original state after ethanol is fully evaporated. Such solvent-accelerated recovery process was observed in all the mPI-aGA composites and almost every sample recovered to ~100%.

As discussed above, the morphology recovery of mPI-aGA assisted by ethanol infiltration was mainly due to the good solvent uptake capability of aGA ascribed to the abundant porosity. Though the adsorption capacity of mPI-aGA toward various organic solvents was lower than that of pristine aGA, mPI-aGA still showed fairly good adsorption capability, indicating the introduced PI in mPI-aGA does not significantly reduce the total pore volume (Fig. S2a and Table S2 in Supporting information). Due to different hydrophilic/hydrophobic property, polarity *etc.*, mPI_{60}-aGA_9 exhibited different adsorption capacity for the tested solvents from that of aGA_9. It is worth mentioning that the adsorption rate of mPI-aGA is very fast and similar to the pristine aGA. The rapid uptake of a large amount of the solvent in mPI-aGAs further supports that the polyimine is coated as thin layers on the surface of aGA without significantly occupying the pores of the aGAs, thus causing no obvious decrease in the porosity of aGA [13].

The mPI-aGA composites also exhibit excellent durability. As shown in Fig. 3a, the compressive properties of mPI_{60}-aGA_9 barely changed even after 3000 consecutive compression cycles. Such durability is significantly higher than polyimide/GA composite, which showed >14% reduction of the stress at the 10^{th} cycle under 50% strain [15]. mPI-aGA composites show not only much better durable compressibility but also reparability and sustainability. In practical applications, it is very common that damages, such as wrinkles or shedding, occur in the composites by repeated use and/or over-compression. Such damages not only affect the durability, but also the lifetime and sustainability of the materials, which has not been well addressed for most reported composites [15,35,36]. The effect of the cracks on material performance was demonstrated using mPI_{60}-aGA_9. A crack (length × width × depth = 7 mm × 0.5 mm × 10 mm) was created using a carving blade. The cross cracks in the bottom surface directly reduced the compressive strength of the composite by half (0.16 MPa for cracked composite *vs.* 0.33 MPa for original composite) under 50% strain (Fig. S3a in Supporting information). The compressive strength of the composite dropped significantly (5-fold difference) to 0.06 MPa in the 22nd test (Fig. S3a). The sample with the crack at the lateral side showed the continuous decrease of the compressive strength during the first 13 tests (Fig. S3b in Supporting information). These results clearly show the detrimental effect of such small cracks on the durability of the mPI_x-aGA_y composites. Due to the interconnected 3D network of conductive graphene sheets in the composite, the creation of the cracks did not show obvious immediate effect on the conductivity of mPI_{60}-aGA_9 (Fig. S3c in Supporting information).

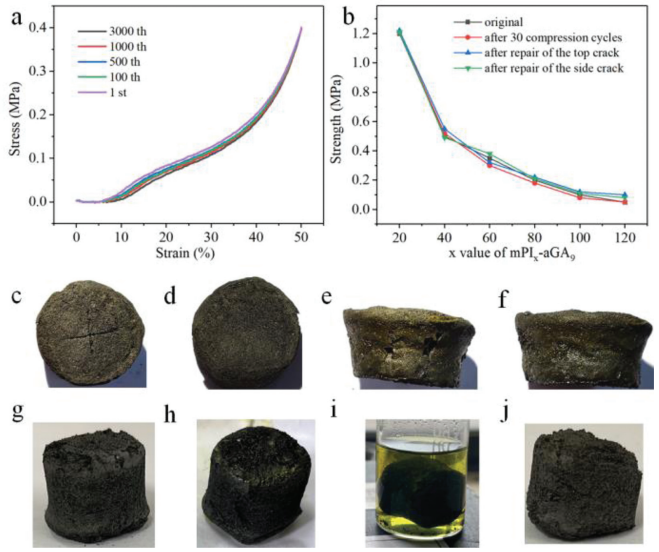

Fig. 3. (a) The stress-strain curves of mPI_{60}-aGA_9 under 3000 consecutive compression cycles; (b) compressive strength of mPI-aGA_9 composites at different states under 50% strain. Optical images of mPI_{60}-aGA_9 with cracks and after repairing: a sample with a crack (c) in the bottom and (d) after repair and a sample with a crack (e) on the side and (f) after repair. Optical images of aGA_9 and mPI_{60}-aGA_9 during the recycling process: (g) the as-prepared aGA_9 and (j) recycled aGA_9, mPI_{60}-aGA_9 (h) before and (i) during the recycling process (the yellow color results from dissolved imine oligomers).

The reversibility of imine bonds in the polyimine matrix can enable the repairing and rehealing of the mPI-aGA composites. A cross-crack (length × width × depth = 7 mm × 0.5 mm × 10 mm) made in the bottom or the surface of the lateral side of mPI_{60}-aGA_9 sample could be easily repaired by simply "wrapping" the cylindrical mPI-aGA with a copper wire and then heating it at 65 °C for 2 h after filling in a small amount of solvent (DMF) into the crack (details shown in Experimental procedures in Supporting information). As shown in Figs. 3c–f, no obvious crack was observed after healing, supporting that the crack was fully rehealed. To further confirm the healing capability and evaluate its efficiency, the mechanical properties of the repaired samples (with crack in the bottom or at the lateral side) were investigated. As shown in Fig. 3b, the repaired samples exhibit nearly the same compressive strength as the original sample, demonstrating the high (close to 100%) healing efficiency. Some composites, *e.g.*, mPI_{40}-aGA_9 and mPI_{120}-aGA_9, even exhibited slightly improved compressive strength after repair. As the solvent (DMF here) can modulate the rate of the imine bond exchange (catalyzed by the residual dangling primary amine in the network) and thus the dynamical properties of the composite [37], the improved compressive strength is possibly due to the reorganization of polyimine cross-linking networks in GA, which could result in a more uniform distribution of polymers throughout the monolithic aerogel than before. Furthermore, the repaired mPI_{60}-aGA_9 displayed strong durability comparable to the original one, showing similar stress-strain curves for 3000 consecutive cycles (Fig. S3d in Supporting information). SEM characterization (Figs. S4 and S5 in Supporting information) of mPI_{60}-aGA_9 confirmed there was no obvious morphology change after the durability test, *i.e.*, PI is still wrapped on the surface of graphene sheet but accompanied by some degree of aggregation. The interface rehealability also gives mPI-aGAs the ability to reshape and weld. A cylindrical mPI-aGA sample can be cut into different shapes, which can be then welded together to form a more complicated 3D shape (Fig. S6 in Supporting information).

Other than being easy to repair and reheal, the mPI-aGA composites can also be easily recovered (fully recyclable) *via* the tran-

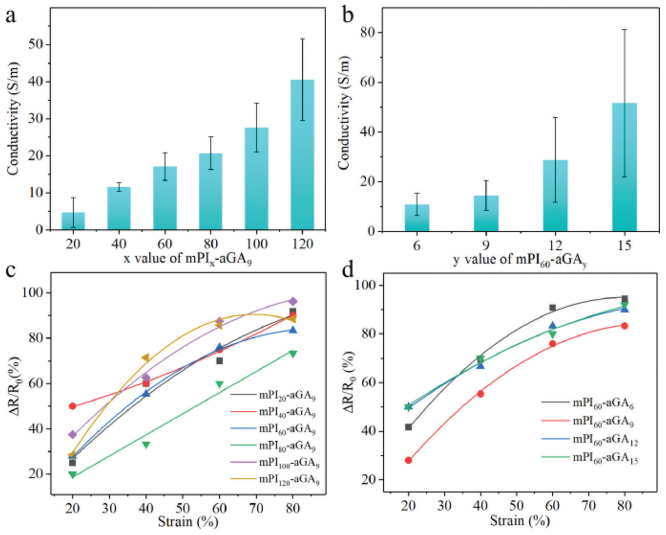

Fig. 4. Conductivities of (a) mPI$_x$-aGA$_9$ composites and (b) mPI$_{60}$-aGA$_y$ composites. Piezoresistive characteristics (resistance–strain behavior) of (c) mPI$_x$-aGA$_9$ composites and (d) mPI$_{60}$-aGA$_y$ composites.

simination reaction between the excess diamine monomers (*i.e.*, DETA and TREN) and the imine-linked network (Figs. 3g–j). The graphene aerogel composite (*e.g.*, mPI$_{60}$-aGA$_9$) was soaked in the solution of DETA and TREN in 20 mL of DMF. After heating at 65 °C for 8 h, a yellow homogeneous solution was obtained due to the depolymerization of PI binder. The monolithic aerogel could be ~100% recovered by decanting the solution and rinsing the aerogel with ethanol to remove any polymer binder residues (the recovery process could be monitored with FTIR as shown in Fig. S7 in Supporting information). The depolymerization solution (20 mL) can be directly mixed with a DMF solution (40 mL) of complementary monomers to form the next-generation (recycled) mPI-aGA composite material (see Experimental procedures in Supporting information). Remarkably, the obtained recycled mPI-aGA exhibited comparable mechanical property with that of the as-prepared composite (Fig. S8 in Supporting information).

The conductivities of mPI-aGA composites were then investigated as they consist of highly conductive GA. The as-prepared cylindrical composites were cut horizontally into small flat cylinders and then compressed into thin sheets. The conductivities of compressed thin sheets were measured by a four-probe method. Figs. 4a and b show that mPI$_x$-aGA$_y$ composites exhibit different conductivities from 0.2 S/m to 79 S/m depending on the constitutions (*i.e.*, x and y values). We found the conductivities of the composites are directly related to the weight fraction of the conductive component GA in the composites. With the same GA loading (y is fixed to 9), the conductivities of the composites increased with the decrease of the weight fraction of PI (increase of x value) (Fig. 4a). Vice versa, with the same PI weight fraction (x is fixed to 60), the conductivities of the composites increase with the increase of the weight fraction of GA (increase of y value) (Fig. 4b).

The good conductivity and the excellent compressibility of mPI-aGA along with a monolithic architecture prompt us to investigate the resistance change with the applied mechanical strain, which is often referred as piezoresistive properties. The resistance changes of mPI-aGA under different strain rates were obtained *in situ* by using an electrical universal testing machine equipped with a multimeter (Fig. S9 in Supporting information). Figs. 4c and d show the relative resistance variation ($\Delta R/R_0$) at different compression strains of mPI-aGA (ΔR is the change of R from zero-strain (R_0) to an applied strain). The results show that $\Delta R/R_0$ increases with the increase of the compression strain. When the pressure is imposed, the contact area and conduction paths of the microstructure increase, resulting in the decrease of the resistance [38]. For all the samples, the absolute value of $\Delta R/R_0$ increases from 0 (zero strain) to >70% (80% strain) with increasing strain. Some of them (*i.e.*, mPI$_{40}$-aGA$_9$, mPI$_{80}$-aGA$_9$) even show good linear sensitivity. The adjustability of constitution of mPI-aGAs offers a great opportunity to tune such piezoresistive properties to meet the specific needs of sensing in targeted wearable devices. It should be noted that the resistance only changes with the height of mPI-aGA pillar without changing the morphology. The durable compressibility of mPI-aGAs could enable sustainable and accurate piezoelectric-like properties.

In summary, we have prepared cylindrical monolithic polyimine and GA composites (mPI-aGAs) *via* simple infiltration of PI monomers into the pores of GA followed by thermal curing. The obtained mPI-aGAs showed excellent durable compressibility, high adjustable compressive strength and conductivity, which provide mPI-aGAs good piezoresistive properties. Moreover, enabled by the dynamic imine chemistry, mPI-aGAs are rehealable, reproccessable, and fully recyclable. Rehealing with ~100% recovery of the compressive strength and electric conductivity was achieved with simple heating treatment. Such full recovery and recyclability have rarely been reported for electronic materials (*i.e.*, unrepairable and/or rehealable *via* complicated procedures), which can greatly reduce electronic waste and overall production cost. The reported mPI-aGAs therefore show great potential as sensing materials in the field of environmentally friendly and flexible electronics for various applications.

Declaration of competing interest

The authors report no declarations of interest.

Acknowledgments

This work was financially supported by National Natural Science Foundation of China (No. 21875208), Yunnan University (Nos. WX160117, C176220100005), University of Colorado Boulder, High-Level Talents Introduction in Yunnan Province (No. C619300A025), the Key Project of Natural Science Foundation of Yunnan (No. 202201AS070011), Major Science and Technology Project of Precious Metal Materials Genetic Engineering in Yunnan Province (Nos. 2019ZE001-1, 202002AB080001), and International Joint Research Center for Advanced Energy Materials of Yunnan Province (No. 202003AE140001). The authors thank Advanced Analysis and Measurement Center of Yunnan University for the sample testing service.

Supplementary materials

Supplementary material associated with this article can be found, in the online version, at doi:10.1016/j.cclet.2022.03.086.

References

[1] M.B. Bryning, D.E. Milkie, M.F. Islam, et al., Adv. Mater. 19 (2007) 661–664.
[2] B. Qiu, M. Xing, J. Zhang, J. Am. Chem. Soc. 136 (2014) 5852–5855.
[3] M. Sajjad, R. Tao, K. Kang, ACS Appl. Energy Mater. 4 (2021) 828–838.
[4] N. Li, Y. Liu, X. Ji, et al., Chin. Chem. Lett. 32 (2021) 3787–3792.
[5] G. Shao, O. Ovsianytskyi, M.F. Bekheet, A. Gurlo, Chem. Commun. 56 (2020) 450–453.
[6] Q. Li, D. Chen, J. Miao, et al., ACS Appl. Mater. Interfaces 12 (2020) 25243–25252.
[7] T. Zhao, Y. Ren, G. Jia, et al., Chin. Chem. Lett. 30 (2019) 2032–2038.
[8] Z. Wang, R. Wei, J. Gu, et al., Carbon 139 (2018) 1126–1135.
[9] F. Sun, Q. Liu, Y. Xu, et al., Chem. Eng. J. 415 (2021) 128976.
[10] B. Wang, Q. Wu, Y. Fu, T. Liu, J. Mater. Sci. Technol. 86 (2021) 91–109.
[11] C.H.A. Tsang, J. Tobin, J. Xuan, et al., Appl. Catal. B: Environ. 240 (2019) 50–63.
[12] J. Li, Q. Wang, L. Zheng, H. Liu, J. Mater. Sci. Technol. 41 (2020) 68–75.

[13] H. Hu, Z. Zhao, W. Wan, Y. Gogotsi, J. Qiu, ACS Appl. Mater. Interfaces 6 (2014) 3242–3249.
[14] H. Hu, Z. Zhao, R. Zhang, Y. Bin, J. Qiu, J. Mater. Chem. A 2 (2014) 3756–3760.
[15] J. Huang, J. Wang, Z. Yang, S. Yang, ACS Appl. Mater. Interfaces 10 (2018) 8180–8189.
[16] M. Wang, X. Duan, Y. Xu, X. Duan, ACS Nano 10 (2016) 7231–7247.
[17] Y. Jin, Z. Lei, P. Taynton, S. Huang, W. Zhang, Matter 1 (2019) 1456–1493.
[18] M.K. McBride, B.T. Worrell, T. Brown, et al., Annu. Rev. Chem. Biomol. Eng. 10 (2019) 175–198.
[19] M. Guerre, C. Taplan, J.M. Winne, F.E. Du Prez, Chem. Sci. 11 (2020) 4855–4870.
[20] B. Krishnakumar, R.V.S.P. Sanka, W.H. Binder, et al., Chem. Eng. J. 385 (2020) 123820.
[21] P. Taynton, K. Yu, R.K. Shoemaker, et al., Adv. Mater. 26 (2014) 3938–3942.
[22] Y. Xu, K. Odelius, M. Hakkarainen, ACS Sustain. Chem. Eng. 8 (2020) 17272–17279.
[23] K. Liang, G. Zhang, J. Zhao, et al., ACS Sustain. Chem. Eng. 9 (2021) 5673–5683.
[24] Z. Zou, C. Zhu, Y. Li, X. Lei, J. Xiao, Sci. Adv. 4 (2018) eaaq0508.
[25] J. Zhang, Z. Lei, S. Luo, et al., ACS Appl. Nano Mater. 3 (2020) 4845–4850.
[26] C. Shi, Z. Zou, Z. Lei, et al., Sci. Adv. 6 (2020) eabd0202.
[27] S. Luo, Y. Ma, X. Wei, et al., ACS Appl. Electron. Mater. 3 (2021) 1178–1183.
[28] J.Y. Hong, E.H. Sohn, S. Park, H.S. Park, Chem. Eng. J. 269 (2015) 229–235.
[29] M. Weigel, J. Steimle, Proc. ACM Interact. Mob. Wearable Ubiquitous Technol. 1 (2017) 28.
[30] G. Shan, X. Li, W. Huang, Innovation 1 (2020) 100031.
[31] H. Jin-Yong, M.B. Bo, J.J. Wie, K. Jing, H.S. Park, Adv. Funct. Mater. 25 (2015) 1053–1062.
[32] H. Ha, K. Shanmuganathan, C.J. Ellison, ACS Appl. Mater. Interfaces 7 (2015) 6220.
[33] Y. Qin, Q. Peng, Y. Ding, et al., ACS Nano 9 (2015) 8933–8941.
[34] H. Sun, Z. Xu, C. Gao, Adv. Mater. 25 (2013) 2554–2560.
[35] Z. Wang, X. Shen, N.M. Han, et al., Chem. Mater. 28 (2016) 6731–6741.
[36] G. Tang, Z.G. Jiang, X. Li, et al., Carbon 77 (2014) 592–599.
[37] A. Chao, I. Negulescu, D. Zhang, Macromolecules 49 (2016) 6277–6284.
[38] W. Yao, R. Mao, W. Gao, et al., Carbon 158 (2020) 418–425.